

Lattice Theory of Pseudospin Ferromagnetism in Bilayer Graphene: Competing Orders and Interaction Induced Quantum Hall States

Jeil Jung,* Fan Zhang, and Allan H. MacDonald
Department of Physics, University of Texas at Austin, USA
(Dated: June 8, 2018)

In mean-field-theory bilayer graphene's massive Dirac fermion model has a family of broken inversion symmetry ground states with charge gaps and flavor dependent spontaneous inter layer charge transfers. We use a lattice Hartree-Fock model to explore some of the physics which controls whether or not this type of broken symmetry state, which can be viewed as a pseudospin ferromagnet, occurs in nature. We find that inversion symmetry is still broken in the lattice model and estimate that transferred areal densities are $\sim 10^{-5}$ electrons per carbon atom, that the associated energy gaps are $\sim 10^{-2}eV$, that the ordering condensation energies are $\sim 10^{-7}eV$ per carbon atom, and that the energy differences between competing orders at the neutrality point are $\sim 10^{-9}eV$ per carbon atom. We explore the quantum phase transitions induced by external magnetic fields and by externally controlled electric potential differences between the layers. We find, in particular, that in an external magnetic field coupling to spontaneous orbital moments favors broken time-reversal-symmetry states that have spontaneous quantized anomalous Hall effects. Our theory predicts a non monotonic behavior of the band gap at neutrality as a function of interlayer potential difference in qualitative agreement with recent experiments.

PACS numbers: 71.10.-w, 71.15.Nc, 71.15.Ap, 73.22.Gk, 73.22.Pr, 73.43.-f

I. INTRODUCTION

Recent experimental progress^{1,2} in isolating and measuring the electronic properties of graphene single and multilayers has opened a new topic in two-dimensional electron system (2DES) physics³. Electronic wavefunctions in graphene systems are often described using a pseudospin language in which the spinors specify wavefunction components on different sublattices. Although the properties of graphene 2DES's can often be successfully described using an effective non-interacting electron model, studies of electron-electron interactions effects have revealed some qualitative differences compared to ordinary 2DES's^{4,5} that are related to these sublattice pseudospin degrees-of-freedom.

In the case of AB stacked bilayer graphene, there are four C sites and four π -orbitals per unit cell, but two of these are repelled from the neutral system Fermi level by interlayer hopping. This circumstance leads to a low-energy massive chiral fermion model⁶ with two-component spinors, and a crystal-momentum \vec{p} dependent pseudo-magnetic field with a magnitude that varies as p^2 and an orientation angle twice as large as the momentum orientation angle $\phi_{\vec{p}}$. Neutral system states have one occupied pseudospin for each distinct set of momentum, spin, and valley labels. Recently⁷ Min *et al.* pointed out that when Coulombic electron-electron interactions are added to the massive chiral fermion model, the mean-field theory ground state pseudospins of each spin-valley flavor break symmetry by rotating out of the $x-y$ plane, developing \hat{z} components with a common spontaneously chosen sign and magnitudes which are larger at small p . Because the two-sublattices from which the two-band-model pseudospins are constructed are located in opposite layers, the broken symmetry transfers charge between layers. It is therefore characterized in momentum space by a vortex with vorticity $\nu = 2$ and a flavor-dependent core polarized along one of the polar directions, and in real space by flavor-dependent uniform layer polarization. Different members of the family of states are dis-

tinguished by the spin-valley flavor dependence of the sense of layer pseudospin orientation in the momentum-space vortex cores. The origin of the broken symmetry, which we refer to here as pseudospin ferromagnetism,⁷ is the p^2 pseudospin-splitting at small p , which leads to infrared divergences⁸ in particle-hole polarization loops, combined with the frustrating effect of pseudospin chirality which leads to relatively stronger exchange interactions for \hat{z} -polarized pseudospins.

The broken symmetry states can be classified^{9,10} in a manner which highlights their valley and spin dependent momentum space Berry curvatures, which are in turn closely related^{11,12} to the Hall responses of the system. Indeed, recent experiments¹³ demonstrate that bilayer graphene exhibits a quantized quantum Hall effect in the absence of an external magnetic field. Over and above the basic science interest deriving from this presently unique property, it is possible that pseudospin order in bilayer graphene could play a role in graphene electronics¹⁴ by introducing hysteresis and dramatically enhancing the influence of gates on conductance.

In this article we report on a study of pseudospin ferromagnetism in a π -orbital tight-binding model for bilayer graphene, which is conveniently able to capture and establish the role of some bilayer graphene π -band features neglected in the massive chiral fermion model. We estimate that the density shift for each flavor is $\sim 10^{-5}$ electrons per carbon atom, that the gaps are $\sim 10^{-2}eV$, that the total condensation energy is $\sim 10^{-7}eV$ per carbon atom, and that the energy differences between competing ordered states is $\sim 10^{-9}eV$ per carbon atom. The energy differences between competing ordered states, which are between one to two orders or magnitude smaller than the condensation energy, are sensitive to roughly estimated lattice scale details of the model we employ. The competing states are classified in the first place as either anomalous Hall states, in which opposite valleys are polarized toward opposite layers, or valley Hall states in which they are polarized toward the same layer. We find that valley Hall states have slightly lower energies. Because anoma-

lous Hall states have spontaneous orbital magnetism they are favored by external magnetic fields. We estimate that, because the energy differences between states are very small, extremely weak fields are sufficient to induced phase transitions between valley Hall and anomalous Hall states. On the other hand potential differences between layers favor valley Hall states. When the spin degree of freedom is accounted for we find that the spontaneous energy gap in neutral bilayers first decreases and then increases with potential difference, in qualitative agreement with experiment.

In the following two sections we explain the model Hamiltonian we employ and some of the technical details of the calculations we have carried out. The main results are presented in the Section IV where we introduce the topological classification of solutions and use it to discuss the properties of broken symmetry solutions for vanishing, moderate, and strong externally controlled electric potential differences between the layers. (Below we refer to interlayer potential differences, which always play a key role in graphene bilayer physics, as potential biases.) We also discuss coupling to an external magnetic field which can drive transitions between competing states, some of which have broken time-reversal-symmetry with associated anomalous Hall effects and orbital magnetism.

We close the paper with a summary and some suggestions for further research.

II. FOUR-BAND π -ORBITAL TIGHT-BINDING MODEL OF BILAYER GRAPHENE

We describe bilayer graphene using a lattice model with one atomic $2p_z$ orbital per carbon site. We write the model's Bloch basis states in the form

$$\psi_{\mathbf{k}\kappa}(\mathbf{r}) = \frac{1}{\sqrt{N}} \sum_i e^{i\mathbf{k}(\mathbf{R}_i + \boldsymbol{\tau}_\kappa)} \phi(\mathbf{r} - \mathbf{R}_i - \boldsymbol{\tau}_\kappa), \quad (1)$$

where N is the total number of unit cells in the system, $\phi(\mathbf{r})$ is the band's Wannier wavefunction, and κ labels the carbon site with position $\boldsymbol{\tau}_\kappa$ relative to a the triangular lattice vector \mathbf{R}_i . (We comment later on the possible role of screening effects from the p and s orbitals which form the σ and σ^* bonds neglected in this model.) Following the convention used in Refs.[6,15], we use the notations $A, B, \tilde{A}, \tilde{B}$ for the four sublattice indexes κ , where B and \tilde{A} are the opposite-layer near-neighbor-pair sites. With this convention, the four band tight-binding model Hamiltonian of a graphene bilayer is:

$$H_0 = \begin{pmatrix} 0 & \gamma_0 f & \gamma_4 f & \gamma_3 f^* \\ \gamma_0 f^* & 0 & \gamma_1 & \gamma_4 f \\ \gamma_4 f^* & \gamma_1 & 0 & \gamma_0 f \\ \gamma_3 f & \gamma_4 f^* & \gamma_0 f^* & 0 \end{pmatrix} \quad (2)$$

where

$$f(\mathbf{k}) = e^{ik_y a / \sqrt{3}} \left(1 + 2e^{-i3k_y a / 2\sqrt{3}} \cos\left(\frac{k_x a}{2}\right) \right) \quad (3)$$

with $a = 2.46\text{\AA}$ arises from a sum over the three near-neighbor hops within a layer. We have neglected differences in on-site energies and next nearest neighbor hopping processes which give rise to electron-hole asymmetry and do not play an important role in pseudospin ferromagnetism. The tight-binding model parameters γ_i should not be confused with the Slonczewski-Weiss, McClure¹⁶ model parameters for bulk graphite, despite the obvious similarities in notation. In our calculations we adopt conventions similar to those of Ref.[17] for bilayer graphene, taking the values $\gamma_0 = -3.12\text{ eV}$, $\gamma_1 = -0.377$, $\gamma_3 = -0.29\text{ eV}$ and $\gamma_4 = -0.12\text{ eV}$ for the hopping parameters. Only the intralayer nearest neighbor (γ_0) process and interlayer tunneling (γ_1) process are retained in the minimal tight-binding model. The trigonal warping (γ_3) process which connects the A and \tilde{B} sites is responsible for the leading circular symmetry breaking near the valley points, while the (γ_4) process which connects A and \tilde{A} sites influences the intralayer charge imbalance between sublattices A and B .

III. LATTICE MODEL MEAN-FIELD THEORY

Because of the importance⁵ of non-local exchange in graphene systems, a Hartree-Fock mean-field theory approximation¹⁸ is a natural first step in considering electron-electron interaction effects. When Coulomb interactions are added to the π -band tight-binding model the interaction terms in the mean-field Hamiltonian take the form:

$$V^{HF} = \sum_{\mathbf{k}\lambda\lambda'} U_H^{\lambda\lambda'} N_{\lambda'} c_{\mathbf{k}\lambda}^\dagger c_{\mathbf{k}\lambda} - W_{\mathbf{k}\lambda\lambda'}^X c_{\mathbf{k}\lambda}^\dagger c_{\mathbf{k}\lambda'} \quad (4)$$

where λ is a composite label for sublattice κ and spin σ . The first term on the right hand side of Eq. (4) is the Hartree term:

$$N_\lambda = N_{\kappa\sigma} = \sum_{\mathbf{k}'} \langle c_{\mathbf{k}'\lambda}^\dagger c_{\mathbf{k}'\lambda} \rangle = \sum_{\mathbf{k}'} n_{\mathbf{k}'\lambda} \quad (5)$$

$$U_H^{\lambda\lambda'} = \frac{\delta_{\sigma,\sigma'}}{A} \sum_{\mathbf{G}} \exp[i\mathbf{G}(\boldsymbol{\tau}_\kappa - \boldsymbol{\tau}_{\kappa'})] \left| \tilde{f}(|\mathbf{G}|) \right|^2 V^{\kappa\kappa'}(|\mathbf{G}|), \quad (6)$$

where \mathbf{G} is a reciprocal lattice vector. The second is the Fock (exchange) term:

$$W_{\mathbf{k}\lambda\lambda'}^X = \sum_{\mathbf{k}'} U_X^{\kappa\kappa'}(\mathbf{k}' - \mathbf{k}) \langle c_{\mathbf{k}'\lambda'}^\dagger c_{\mathbf{k}'\lambda} \rangle \quad (7)$$

$$U_X^{\kappa\kappa'}(\mathbf{q}) = \frac{1}{A} \sum_{\mathbf{G}} \exp[i\mathbf{G}(\boldsymbol{\tau}_\kappa - \boldsymbol{\tau}_{\kappa'})] \times \left| \tilde{f}(|\mathbf{q} - \mathbf{G}|) \right|^2 V^{\kappa\kappa'}(|\mathbf{q} - \mathbf{G}|). \quad (8)$$

In Eq.(6) and Eq.(8) the two-dimensional Coulomb interaction $V^{\kappa\kappa'}(\mathbf{q}) = 2\pi e^2 / (|\mathbf{q}| \epsilon_r)$ when κ and κ' refer to the same layer and $(2\pi e^2 / (|\mathbf{q}| \epsilon_r)) \exp[-|\mathbf{q}|c]$ when κ and κ' refer to the opposite layers. Here ϵ_r is the relative dielectric constant, $c = 3.35\text{\AA}$ is the interlayer separation, A is the total area of the graphene sheet, and we use

$$\tilde{f}(q) = (1 - (r_0 q)^2) / ((1 + (r_0 q)^2)^4) \quad (9)$$

as a form factor which accounts for the spread of the π -orbital charge on each site. This simple form assumes an isotropic site-localized charge distribution. Eq. (9) was obtained by Fourier transforming the radial charge distribution of a hydrogenic $2p$ orbital. The use of $r_0 = \bar{a}_0 = a_0/\sqrt{30}$ would yield a root mean square radius corresponding to the covalent radius of the carbon atom $a_0 = 0.77\text{\AA}$. If we consider screening from the σ band electrons neglected in our model and the fact that the charge density distribution of a p_z orbital is far from spherical we expect that larger values of r_0 , which effectively reduce onsite repulsion, would be more appropriate. For most of our calculations we have therefore used the value $r_0 = 3\bar{a}_0$.

As explained in the introduction, pseudospin ferromagnetism in bilayer graphene can be neatly described using the two-band massive chiral fermion model. This approach has two shortcomings which the present calculation is intended to alleviate. First of all, the model has to rely on a crude ultraviolet-cutoff to account for the limited range of energy $\sim \gamma_1$ over which it is applicable. At moderate interaction strengths the amount of charge transferred between layers determined in the massive chiral fermion model calculation is strongly influenced by this cut-off. Secondly, the calculation described in Ref. (7) relies on the model's circular symmetry for a number of simplifications. When direct hopping between the low-energy A and \bar{B} sites, the γ_3 process, is included in the Hamiltonian the model's Fermi lines are no-longer circular and the continuum model loses some of its attractive simplicity.^{19,20} These processes are known to be essential at very weak interaction strengths since they remove the infrared divergences^{8,21} responsible for the instabilities of the massive chiral fermion model. The present lattice model reduces to the continuum model at low energies, accounts naturally for the limited validity range of two-band models by retaining all four π -bands, and can deal with the loss of circular symmetry without any additional complication.

The main challenges which arises in practical implementation of the lattice model mean-field-theory lie in the numerical optimization of a problem in which the small portion of the Brillouin-zone close to one of the valley points plays a dominating role and must be sampled densely. It is essential that we have sufficiently dense k -point sampling near the Dirac points, and at the same time sample the full Brillouin zone. The increase of computational load with k -point sampling density is particularly rapid in the Hartree-Fock calculations because the Hartree-Fock matrix element at one k -point depends on the occupied wavefunctions at all other k -points. In Fig. 1 we illustrate the honeycomb lattice reciprocal space primitive cell and the k -point sampling scheme we have chosen. In an effort to achieve a satisfactory compromise between computational load and accuracy we, first of all, make use of the hexagonal symmetry inherent in the problem. This allows us to limit our calculations to 1/6th of the total Brillouin zone area when we distinguish K and K' valleys, and 1/12th of the total area when we do not. In addition, instead of using a uniform grid in the whole Brillouin zone we use a k -point mesh which is denser near the Dirac point. In our calculations we have used 18×18 , 32×32 or 42×42 coarse grids for the full primitive cell and multiplication factors of up to 128 for

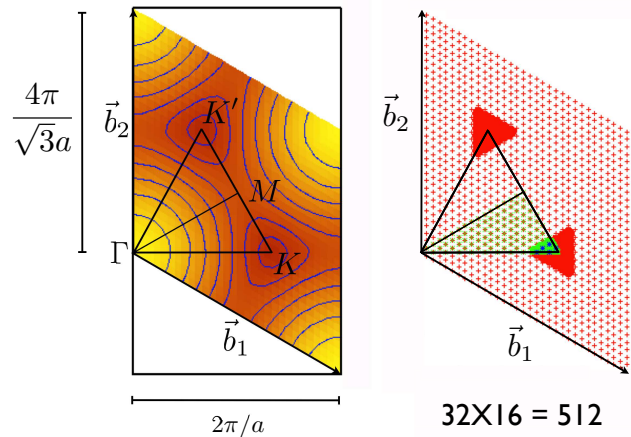


FIG. 1: *Left panel:* Band structure of graphene represented in the primitive zone defined by the reciprocal lattice vectors \vec{b}_1 and \vec{b}_2 of the honeycomb lattice. The equilateral triangle represents the region in the primitive cell we need to sample in order to fully describe a system in which the symmetry between K and K' valleys is broken. The smaller triangles enclose inequivalent regions in k -space associated with K and K' valleys. *Right panel:* An example of coarse sampling of k -points in the primitive cell supplemented by a finer grid in hexagons generated around those coarse k -points near the K and K' valleys. The illustrated example consists of 32×32 coarse points and a 16-fold enhancement of density resulting in an effective sampling of 512×512 points in the primitive cell near the valleys.

the finer k -point mesh near the valley centers. The fine mesh densities were either 2304×2304 or 2048×2048 for typical calculations at zero potential bias, and 672×672 when smaller densities were enough to converge the calculations in the case of strongly biased bilayers. Dense k -point meshes were normally employed within $\sim 0.5/a$ of a Dirac point, and wider regions were used for strong bias cases. (Here $a = 2.46\text{\AA}$ is the lattice constant of the triangular periodic lattice structure of graphene.) Nevertheless k -point sampling approximations remain the main source of numerical inaccuracies. The self-consistent-field calculations were iterated until convergence to 14 significant figures in the total energy per electron was achieved for a given choice of k -point sampling. In order to resolve the small energy differences between solutions of the self-consistent field equations corresponding to different states we needed to compare results obtained with the same k -point sampling scheme. The k -point sampling we used achieved convergence to within a few parts per thousand for charge density differences and band gaps.

IV. LATTICE MODEL PSEUDOSPIN FERROMAGNET

The inversion symmetry breaking instability in bilayer graphene occurs nearly independently at the two points and, within mean-field-theory, entirely independently for each electron spin.⁷ It is strongest in electrically neutral

bilayers.^{8,15,21,23} Initial studies carried out at the Hartree-Fock level⁷ identified a family of competing pseudospin ferromagnet states. Perturbative renormalization group calculations^{8,21,22} have confirmed that these instabilities can survive beyond mean-field-theory.

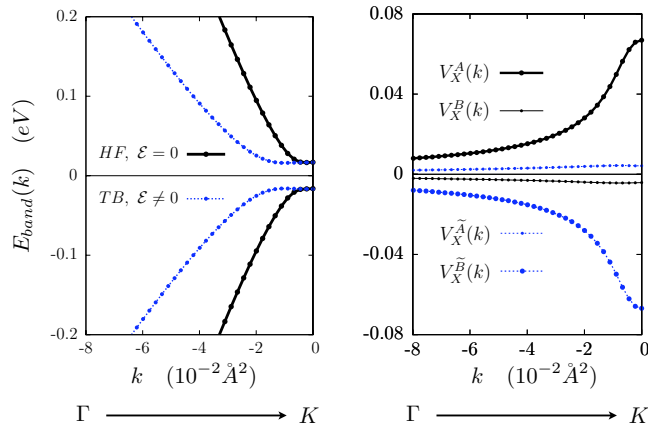


FIG. 2: *Left panel:* Non-interacting biased tight-binding model (dotted line) and unbiased Hartree-Fock (solid line) band structures for bilayer graphene for k moving away from the Γ point towards the Dirac point K . The broken symmetry state bands are compared with non-interacting electron bands with inversion symmetry explicitly broken by an externally applied electric field $\mathcal{E} = 0.1V/nm$. The interacting system bands exhibit enhanced velocities and a band gap due to spontaneously broken inversion symmetry. These results were obtained for a model with hopping parameters $\gamma_0 = -3.12eV$, $\gamma_1 = -0.377eV$, $\gamma_3 = \gamma_4 = 0$, and dielectric screening parameter $\epsilon_r = 4$. *Right panel:* Onsite k -dependent exchange potentials of the spontaneously broken symmetry state on the four bilayer sublattices. The onsite potential is larger in magnitude on the low-energy sites that do not have an opposite layer neighbor, and lower on average in the layer with the larger density.

Fig. 2 illustrates typical mean-field theory band structures for a π -band tight-binding model of unbiased bilayer graphene. The non-interacting bands exhibit the p^2 dispersion at small p which is captured by the massive chiral fermion model. When interaction effects are included in the mean-field Hamiltonian, a gap opens up and velocities increase substantially. The gap to the remote bands associated with the high energy states is also increased. A gap at $p = 0$ (where $\mathbf{k} = \mathbf{K}$ so that $f(\mathbf{k})$ vanishes) is always associated with a difference in mean-field atomic π -orbital energies between the two low-energy sites A and \tilde{B} and therefore a violation of the inversion symmetry which makes the two layers equivalent. We refer to this broken symmetry state as a pseudospin ferromagnet, motivated by its continuum model description⁷ in which the sublattice degree-of-freedom plays the role of a pseudospin. The increase in velocity at non-zero p illustrated in Fig. 2 occurs even when inversion symmetry is not broken²⁵. In the same figure we plot the k -dependent onsite exchange potentials of the broken symmetry state which

have been obtained from the self consistent solutions. The exchange potentials have opposite signs on opposite layers, larger magnitude at the low energy sites A and \tilde{B} , and values that increase as the valley points are approached.

It is appropriate at this point to address some of the difficulties which arise in constructing reliably predictive theories for the influence of electron-electron interactions in graphene sheets. In continuum model theories it is customary to introduce a relative dielectric constant $\epsilon_r \sim (\epsilon_{sub} + 1)/2$ to account for dielectric screening due to the substrate on which the graphene sheet lies. (ϵ_{sub} is the dielectric constant of the substrate. $\epsilon_{sub} \sim 4$ for substrates commonly used to support mechanically exfoliated graphene samples. This effect is important for some graphene sheet properties but is often omitted in *ab initio* calculations.) Some of the results we present below suggest that the continuum model is reliable, even for neutral graphene systems (which have less screening) and even when ϵ_r is small, as it should be in a model intended to describe suspended graphene samples and in models of graphene on a substrate with a small dielectric constant. As we explain later, the two-band continuum model tends to be less accurate for bilayer graphene than for single-layer graphene. The implication for the lattice model employed here, is that the on-site Coulomb interaction, determined by the charge form factor, will have a bearing on the model's predictions especially when ϵ_r is small. Hartree-Fock mean-field theory, used in this paper to capture the non-local exchange properties which drive pseudospin ferromagnetism, tends to overestimate the onset of broken symmetries. In *ab initio* calculations it is common⁴³ to reduce the strength of bare exchange, say by factor of ~ 2 , to account for Coulomb correlation screening missing in an exchange only theory. This type of consideration may justify using a value of ϵ_r larger than the one which would be suggested by dielectric screening considerations alone, adding another level of uncertainty to any quantitative predictions.

A. Total layer density and Chern number classifications of competing states

Because each bilayer flavor can polarize toward either of the two layers, there are a total number of $2^4 = 16$ possible configurations of the broken symmetry²⁶ state. The layer polarization for each spin and valley determines the sign of the mass term in its continuum model and has implications for the topological properties in the system as we will now discuss. The 16 states can be classified⁷ by overall layer polarization as being ferromagnetic, ferrimagnetic, or layer antiferromagnetic. By this classification⁷ there are two layer ferromagnetic states in which all flavors choose the same polarization, eight layer ferrimagnetic states in which three of the four flavors choose the same polarization, and six layer antiferromagnetic states with no overall polarization.¹⁰ The layer antiferromagnetic states are electrostatically favored in the absence of a potential bias.

One of the most interesting properties of gapped bilayer graphene is the existence of a finite Hall conductivity and orbital magnetism due to the flavor-dependent momentum-space

TABLE I: Summary of Hall transport properties for valley $\tau_z = K, K'$ and spin $\sigma_z = \uparrow, \downarrow$ dependent layer polarization $\lambda_z = T, B$. These states are classified as layer ferromagnetic (F), layer ferrimagnetic (Fi) or layer antiferromagnetic (AF) following reference [7,10]. F, Fi, and AF states have respectively four, three, and two valley-spin components polarized toward the same layer ($\lambda_z = T$). We have listed only eight out of a total of sixteen configurations omitting the equivalent configurations obtained by layer reversal for every flavor. Each valley contributes a finite Hall conductivity with magnitude $\frac{e^2}{h}$ and a sign that reverses with both valley interchange and layer polarization. The Hall conductivities are assigned to particular valleys on the basis of approximate Chern indices obtained by integrating Berry curvatures over the portion of the Brillouin zone near K or K' . The edge-state structure is expected to depend on each of the partial Hall conductivities. The total Hall conductivity is separated into contributions from separate spins and separate valleys using $\sigma_{xy}^{tot} = \sigma_{xy}^{\uparrow} + \sigma_{xy}^{\downarrow} = \sigma_{xy}^K + \sigma_{xy}^{K'}$. The F configuration have zero total hall conductivity, whereas all Fi configurations have a finite total anomalous Hall conductivity of two units. The A configurations are expected to be electrostatically favored in the absence of an external layer bias potential and include three types of solutions with different Hall properties, one with a total anomalous total Hall conductivity, one with zero Hall conductivity but finite spin Hall conductivity, and another with zero Hall and spin Hall conductivities because of opposite Hall conductivity contributions from K and K' valleys for both spins.

	$(\lambda_z \tau_z \sigma_z)$				$\sigma_{xy}^{K,\uparrow}$	$\sigma_{xy}^{K',\uparrow}$	$\sigma_{xy}^{K,\downarrow}$	$\sigma_{xy}^{K',\downarrow}$	σ_{xy}^{\uparrow}	σ_{xy}^{\downarrow}	σ_{xy}^K	$\sigma_{xy}^{K'}$	σ_{xy}^{tot}
F	$(TK\uparrow)$	$(TK'\uparrow)$	$(TK\downarrow)$	$(TK'\downarrow)$	1	-1	1	-1	0	0	2	-2	0
Fi	$(TK\uparrow)$	$(TK'\uparrow)$	$(TK\downarrow)$	$(BK'\downarrow)$	1	-1	1	1	0	2	2	0	2
	$(TK\uparrow)$	$(TK'\uparrow)$	$(TK'\downarrow)$	$(BK\downarrow)$	1	-1	-1	-1	0	-2	0	-2	-2
	$(TK\uparrow)$	$(BK'\uparrow)$	$(TK\downarrow)$	$(TK'\downarrow)$	1	1	1	-1	2	0	2	0	2
	$(TK'\uparrow)$	$(BK\uparrow)$	$(TK\downarrow)$	$(TK'\downarrow)$	-1	-1	1	-1	-2	0	-2	0	-2
AF	$(TK\uparrow)$	$(BK'\uparrow)$	$(TK\downarrow)$	$(BK'\downarrow)$	1	1	1	1	2	2	2	2	4
	$(TK\uparrow)$	$(BK'\uparrow)$	$(TK'\downarrow)$	$(BK\downarrow)$	1	1	-1	-1	2	-2	0	0	0
	$(TK\uparrow)$	$(TK'\uparrow)$	$(BK\downarrow)$	$(BK'\downarrow)$	1	-1	-1	1	0	0	0	0	0

vortices^{9,10,27} in the broken symmetry states. Because the vorticity ν is opposite for opposite valleys, the integrated Berry curvature gives rise to a Hall conductivity^{11,12,28,29} with magnitude e^2/h for each flavor, and a sign that changes with valley as well as with layer polarization. The Berry curvature reflects the handedness of Bloch electrons and captures intracell circulating currents which generate a finite orbital magnetic moment proportional to the angular momentum due to self-rotating Bloch wave packets.²⁹ The Berry curvature of the system can be evaluated using¹¹

$$\Omega_n(\mathbf{k}) = i \sum_{n' \neq n} \left[\frac{\langle u_n | \frac{\partial H}{\partial k_x} | u_{n'} \rangle \langle u_{n'} | \frac{\partial H}{\partial k_y} | u_n \rangle}{(E_{n'} - E_n)^2} - c.c. \right].$$

where $|u_n\rangle$ represents the Bloch eigenstates of the system and E_n are the associated eigenvalues for each k . The finite orbital moment generated by these wave packets has a similar expression and can be evaluated through¹¹

$$\begin{aligned} m_n(\mathbf{k}) &= -(e/2m)L_n(\mathbf{k}) \\ &= -\frac{e}{2\hbar} i \sum_{n' \neq n} \left[\frac{\langle u_n | \frac{\partial H}{\partial k_x} | u_{n'} \rangle \langle u_{n'} | \frac{\partial H}{\partial k_y} | u_n \rangle}{E_{n'} - E_n} - c.c. \right]. \end{aligned}$$

A weak external magnetic field will tend to favor a state in which the orbital magnetizations of all valleys are aligned, and the anomalous Hall conductivity is correspondingly maximized. This observation suggests the possibility of valley optoelectronics that exploits the circular dichroism of interband transitions³⁰ in the broken symmetry states. The Kerr and Faraday effect measurements with linearly polarized light

can be a useful tool to detect signatures of broken time reversal symmetry.⁴⁴ In Fig. 3 we present the k -dependent magnetization evaluated for one self-consistent gapped state in the presence of an interlayer bias. Similar results have been obtained previously using the massive Dirac-fermion continuum model. An estimate of the zero field magnetization per valley-spin degree of freedom $M_{\tau_z \sigma_z} = \sum_n \int m_n(\mathbf{k}) \frac{d^2 \mathbf{k}}{(2\pi)^2} \simeq 2\pi \sum_n \int m_n(k) k \frac{dk}{(2\pi)^2}$ can be obtained integrating the orbital moment around each one of the valleys for a given spin component. For the broken symmetry state with $\varepsilon_r = 4$ each component integrates to $M_{\tau_z \sigma_z} = 10^{-3} \mu_B$ per carbon atom, compared to $M_{\tau_z \sigma_z} = 1.4 \cdot 10^{-3} \mu_B$ for the non-interacting system with bias $\mathcal{E} = 0.1 V/nm$ and $M_{\tau_z \sigma_z} = 2.2 \cdot 10^{-3} \mu_B$ per carbon atom for $\mathcal{E} = 0.4 V/nm$. The individual flavor orbital magnetizations and anomalous Hall contributions cancel in states that do not have broken time-reversal symmetry.

In the non-interacting electron biased bilayer graphene state, opposite contributions from the two valleys lead to vanishing total Hall conductivity, consistent with the absence of broken time-reversal symmetry. The nature of the layer polarized broken symmetry we describe here is analogous to the biased bilayer in the sense that the charge transfer can be attributed to the (k -point dependent) exchange potential difference between low-energy sites on opposite layers, as illustrated in Fig. 2. Because of the non-locality of the exchange interactions, however, we are able to find self-consistent solutions in which the effective interlayer bias potential has opposite signs in the two valleys, and the total Hall conductivity is finite. In Table I we present a list of the 16 different configurations for which we have found self-consistent solutions, which are characterized by the sense of layer ($\lambda_z = T, B$) po-

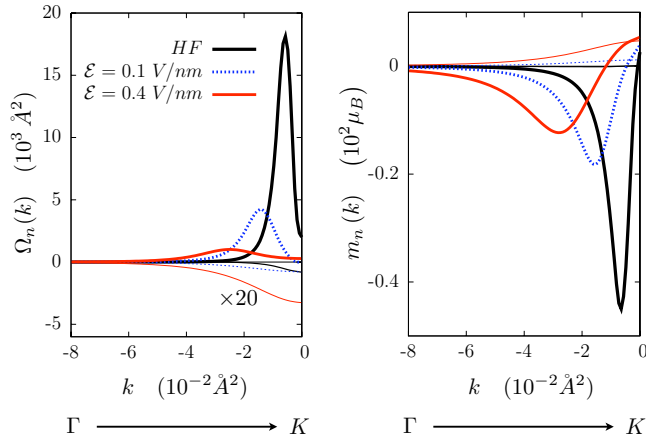


FIG. 3: *Left panel:* Berry curvatures associated with the two valence bands for a Hartree-Fock (HF) solution, and for non-interacting bilayer graphene in the presence of an interlayer bias. We use a thicker line to represent the curvature of the low energy band and a thinner line for the band farther from the Fermi level. The small remote band contribution has been magnified $\times 20$. An interlayer electric field of $\mathcal{E} = 0.1 \text{ V/nm}$ added to the non-interacting electron model gives a band gap comparable to the one which emerges from our mean field calculations with $\epsilon_r = 4$. *Right panel:* Orbital magnetization contributions from the two valence bands in the vicinity of a valley point. We compare results for the self-consistent broken symmetry states with those for non-interacting electrons with an external interlayer bias.

larization for each valley ($\tau_z = K, K'$) and spin ($\sigma_z = \uparrow, \downarrow$) as also discussed in reference [10]. These results suggest the interesting possibility of altering the quantum Hall conductivity of a graphene bilayer sample with an external bias potential as we discuss later.

B. Broken inversion symmetry states in an unbiased bilayer

We start by examining the layer antiferromagnetic charge balanced configurations which are lowest in energy in the absence of an external bias because⁷ of the absence of a Hartree energy penalty. As summarized in Table I, there are three distinct types of layer antiferromagnets.¹⁰ One configuration is the anomalous Hall (AH) state, with four quantized units of Hall conductivity, in which electrons are polarized towards the same layer for both spins⁹, and towards opposite layers for opposite valleys. Second is the spin Hall (SH) state which has opposite layer polarization on opposite valleys, and in each valley opposite layer polarization for opposite spin. The mean-field Hamiltonian for this state is similar to that of a non-interacting system with intrinsic spin orbit coupling³¹. Finally there is a solution with the same layer polarization in the two valleys, but opposite layer polarizations for opposite spins. This state has a finite valley Hall (VH) conductivity for each spin, zero valley Hall conductivity when summed

over spins, and zero total Hall conductivity^{27,32}. Optical measurements based on linearly polarized light using the Kerr and Faraday effect can be used to identify the anomalous Hall state which has broken time reversal symmetry state.⁴⁴

In the continuum model formulation the three distinct solutions are degenerate. In the lattice model Hartree-Fock theory the energies of the AH and SH states are still exactly degenerate because the exchange energy is spin diagonal and the energy within each spin is independent of the Hall effect sign. We refer to these two states collectively as the anomalous Hall states. The valley Hall (VH) solution does have a different energy however, because the relative sense of layer polarization in the two valleys influences inter-valley exchange potentials. Table II presents our results for the condensation energy of the broken symmetry state and for the differences in energy between the VH and AH/SH solutions separated into different contributions. We first note that the condensation energies are reasonably independent of the model parameters ϵ_r and r_0 , which are not precisely known and dependent on the sample's dielectric environment. The scale of the condensation energy should be compared with the value of the Coulomb interaction at the momentum scale k^* ($e^2 k^*$) over which the two-band model applies to bilayer graphene. We find k^* by setting the low-energy model parabolic band energy equal to the isolated layer energy, which gives $k^* \sim \gamma_1 / \hbar v$. The Coulomb energy at this momentum scale is $\sim (e^2 / \epsilon_r \hbar v) \times \gamma_1 = \alpha_{gr} \times \gamma_1 \sim 100 \text{ meV}$. This energy scale gives an estimate of the size of the gap which would be expected if all states with $k < k^*$ were fully layer polarized. We find a gap which is approximately four times smaller and density shifts between layers that are smaller than $\pi k^{*2} / (2\pi)^2 \sim (\gamma_1 / 2\pi W a)^2$ by a similar fraction. These numerical values indicate that the broken symmetry arises mainly from those bilayer band states that are reasonably well described by the low-energy two-band models used in the original mean-field calculations, as expected. We note that the condensation energy is smaller by several orders of magnitude than the total interaction energy, which involves electrons across the full π -band.

The second block of columns present differences in energy between VH states and AH/SH states. For the parameters we have considered the total energies for the VH states are lower than the AH/SH thanks to the exchange energy advantage of the former states. The differences in energy between these states become substantially smaller than the condensation energy when the carbon radius model parameter r_0 is increased. Larger values of r_0 improve the accuracy of the continuum model and differences in energy between the different solutions rapidly decrease. We have previously argued that values of $r_0 \sim 3\tilde{a}_0$ in the form factor are appropriate. If so, the differences in energy between different solutions are $\sim 10^{-9} \text{ eV}$ per carbon atom, about 100 times smaller than the ordering condensation energy. We have also explored an alternative formulation of the Hartree-Fock equations which evaluates the non-local exchange potentials in real space. This formulation allows the model's onsite repulsion U to be adjusted separately from the longer ranged tails^{33,34} and thus allow a more direct assessment of the impact of lattice scale details of the effective Coulomb interaction, and leads to similar conclusions.

TABLE II: Energy differences between distinct mean-field solutions in the absence of a potential bias. The first group of columns represent energy differences between the broken symmetry pseudospin ferromagnet states in the anomalous Hall (AH) configuration and the unbroken symmetry state that has no gap. The latter has been obtained constraining the self-consistent HF calculation to preserve inversion symmetry. The third column represents the exchange energy difference ΔE_X^{TB} of the broken symmetry self-consistent state with respect to the reference exchange energy of the non-interacting state. The remaining columns represent energy differences between anomalous Hall and valley Hall (VH) solutions. The calculated energy differences depend sensitively on the choice of the model parameter r_0 used in the form factor. The total exchange energy differences $\Delta E_X^{tot} = 4(\Delta E_X^{KK} + \Delta E_X^{KK'})$ can be expressed as a sum of intravalley (KK) and intervalley (KK') contributions, where the four-fold factor is due to the twofold degeneracy in both spin and valley. We have verified that the energy differences depend very weakly on the γ_3 and γ_4 parameters which are excluded in the minimal model. The two anomalous Hall states have the same energy in mean-field theory as explained in the text. The values compiled in this Table have been evaluated using $\epsilon_r = 4$ and the indicated carbon atom radii r_0 . All energies are expressed in eV per carbon atom unit.

r_0	$E^{(AH/SH)} - E_0$			$E^{(VH)} - E^{(AH/SH)}$			
	ΔE_{tot}	ΔE_X	ΔE_X^{TB}	ΔE_{tot}	ΔE_X	ΔE_X^{KK}	$\Delta E_X^{KK'}$
\tilde{a}_0	$-4.84 \cdot 10^{-8}$	$-1.13 \cdot 10^{-7}$	$-5.10 \cdot 10^{-4}$	$-1.03 \cdot 10^{-7}$	$-9.72 \cdot 10^{-7}$	$-1.75 \cdot 10^{-7}$	$-6.75 \cdot 10^{-8}$
$2\tilde{a}_0$	$-5.17 \cdot 10^{-8}$	$-1.24 \cdot 10^{-7}$	$-6.15 \cdot 10^{-4}$	$-4.66 \cdot 10^{-9}$	$-1.92 \cdot 10^{-8}$	$-4.09 \cdot 10^{-9}$	$-6.97 \cdot 10^{-10}$
$3\tilde{a}_0$	$-6.17 \cdot 10^{-8}$	$-1.58 \cdot 10^{-7}$	$-5.09 \cdot 10^{-4}$	$-1.14 \cdot 10^{-9}$	$-2.76 \cdot 10^{-9}$	$-5.71 \cdot 10^{-10}$	$-1.18 \cdot 10^{-10}$

TABLE III: Transferred charge per valley-spin flavor in the charge balanced anomalous Hall and valley Hall solutions. In our mean field Hartree-Fock calculations the VH solutions have slightly larger band gaps and interlayer charge transfers than their anomalous Hall counterparts. In this table, charge densities are in units of 10^{11} cm^{-2} and band gaps in meV units. We have used the tight-binding model parameters $\gamma_0 = -3.12 \text{ eV}$, $\gamma_1 = -0.377 \text{ eV}$, $\gamma_3 = -0.29 \text{ eV}$, and $\gamma_4 = -0.12 \text{ eV}$. The γ_3 parameter has only a marginal influence on the broken symmetry state. The value chosen for γ_4 term tends to accumulate more electrons at the low energy sites in the bilayer but does not influence the strength of the broken symmetry. The results reported here were obtained using dielectric constant $\epsilon_r = 4$ and carbon atom radius $r_0 = 3\tilde{a}_0$. In the rightmost set of columns we show the results obtained when a smaller carbon atom radius $r_0 = 2\tilde{a}_0$ is used in the form factor calculation in Eq. (9).

Anomalous Hall / Spin Hall (AH/ SH)																		
ϵ_r	γ_0, γ_1				$\gamma_0, \gamma_1, \gamma_3$				$\gamma_0, \gamma_1, \gamma_3, \gamma_4$				$\gamma_0, \gamma_1, r_0 = 2\tilde{a}_0$					
	Δn_l	Δn_s^A	Δn_s^B	Δ_{gap}	Δn_l	Δn_s^A	Δn_s^B	Δ_{gap}	Δn_l	Δn_s^A	Δn_s^B	Δn_s^A	Δn_s^B	Δ_{gap}	Δn_l	Δn_s^A	Δn_s^B	Δ_{gap}
4	0.52	0.81	-0.29	33	0.52	0.80	-0.28	31	0.52	5.67	-5.15	-4.59	4.07	31	0.47	0.72	-0.25	31
5	0.42	0.60	-0.18	23	0.42	0.60	-0.18	22	0.41	5.38	-4.97	-4.61	4.20	21	0.38	0.54	-0.16	22
6	0.34	0.46	-0.12	17	0.34	0.46	-0.12	16	0.34	5.20	-4.86	-4.63	4.29	16	0.32	0.42	-0.10	16

Valley Hall (VH)																		
ϵ_r	γ_0, γ_1				$\gamma_0, \gamma_1, \gamma_3$				$\gamma_0, \gamma_1, \gamma_3, \gamma_4$				$\gamma_0, \gamma_1, r_0 = 2\tilde{a}_0$					
	Δn_l	Δn_s^A	Δn_s^B	Δ_{gap}	Δn_l	Δn_s^A	Δn_s^B	Δ_{gap}	Δn_l	Δn_s^A	Δn_s^B	Δn_s^A	Δn_s^B	Δ_{gap}	Δn_l	Δn_s^A	Δn_s^B	Δ_{gap}
4	0.52	0.84	-0.32	33	0.52	0.80	-0.28	31	0.52	5.70	-5.18	-4.55	4.03	31	0.49	0.89	-0.40	32
5	0.42	0.61	-0.19	23	0.42	0.61	-0.19	22	0.42	5.40	-4.98	-4.60	4.18	22	0.40	0.64	-0.24	22
6	0.34	0.47	-0.13	17	0.34	0.47	-0.13	16	0.34	5.21	-4.87	-4.62	4.28	16	0.33	0.48	-0.15	17

Large values of U imply strong short-range correlations which are not accurately described by the continuum model. From the results shown in table II, however, we see that only moderate short-range screening from degrees-of-freedom outside the π -band model are required to make deviations from the continuum model small. Given the abundance of separate evidence that interaction effects in graphene systems are accurately described by a continuum model, we assume that the required short-range screening is in fact present.

In Table III we report on the layer distribution of charge when inversion symmetry breaking occurs within a particular valley. The results presented here are single valley-spin re-

sults based on the AH and VH solutions. We have performed these calculations for band models which include and exclude tight-binding hopping parameters other than in plane nearest neighbor hopping γ_0 and interlayer tunneling γ_1 . The trigonal warping γ_3 term connects the sites A and \tilde{B} and introduces a triangular distortion in the band structure near the Dirac point, hence breaking the approximately circular symmetry of the bands. It also makes the dispersion become linear instead of quadratic at the lowest energy scales and works against symmetry breaking. We notice that the reduction of the band gap due to trigonal warping varies between two per cent and ten per cent depending on the short-range interaction strength, in-

dicating that trigonal warping plays a relatively minor role. The γ_4 term increases the accumulation of charge density at lattice sites A and \tilde{B} relative to that at the high energy sites B and \tilde{A} . The gap size and total transferred charge (Δn_l) remain virtually unchanged, although the distribution of charge between sublattices on the same layer ($\Delta n'_s$) is altered in some states.

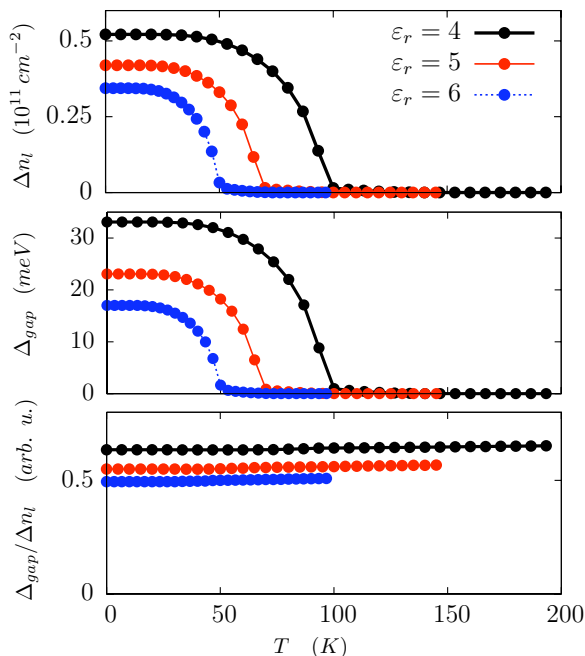


FIG. 4: Temperature dependence of mean-field-theory charge transfer per valley-spin and the associated band gap. *Top panel:* Total charge per unit area (10^{11} cm^{-2}) transferred from one layer to another Δn_l per each valley-spin polarized component as a function of temperature. We represent the dependence for different values of the relative dielectric constant ϵ_r . *Middle panel:* The bottom panel presents the mean-field-theory band gap as a function of temperature. *Bottom panel:* Ratio between the band gap and transferred charge density.

The temperature dependence of the band gap and the transferred charge per valley-spin component in mean-field-theory is plotted in Fig. 4. As the temperature is increased both the charge density and band gaps are reduced, but their ratio is approximately fixed. The decay trend is similar for the different dielectric constants we have considered. The critical temperatures obtained in this mean-field calculation provide an estimate of the maximum temperature at which local order survives in the absence of disorder. The band gap decreases more quickly than the charge-density transfer order parameter as the interaction is made weaker; the charge density per valley-spin varies approximately like ϵ_r^{-1} whereas the gap varies as $\epsilon_r^{-1.55}$.

C. Quantum phase transitions in the low magnetic field and low bias regime

To first order in magnetic field, the magnetic contribution to energy is simply proportional to spontaneous magnetization discussed previously, which is entirely orbital in character and depends on the flavor-dependent layer polarizations. States that are related by layer polarization reversal are no longer equal in energy in the presence of a magnetic field. If we take $\Delta E_{tot} \sim 10^{-9} \text{ eV}$ per carbon atom for the mean field energy differences between AH and VH states from Table II and use the relation $\Delta E_{tot} \sim M_{\tau_z \sigma_z} \cdot B_c$, we obtain from the orbital magnetization values we have calculated that a magnetic field $B_c \sim 0.004 \text{ T}$ is sufficient to favor the AH state with orbital magnetization parallel to the magnetic field over VH states. Considering the small energy differences between the different competing states as shown in table II, we can expect that the coupling between magnetic field and the orbital moment in the system can play a decisive role in selecting the minimum energy ground-state. Because the electron densities at which gaps occur are magnetic field dependent in states with finite Hall conductivity, small fluctuations in the density like those associated with electron-hole puddle domains⁴² will also have an important influence on the nature of the ground-state at low magnetic fields.

We now consider the case of zero magnetic field and finite electric field. In presence of an external bias the inversion symmetry of a graphene bilayer is explicitly broken, favoring charge accumulation in one of the layers. When the external bias becomes large enough the charge balanced broken symmetry antiferromagnetic (AF) configuration gives way to ferrimagnetic (Fi) and eventually ferromagnetic (F) configurations. These solutions can become energetically favored for certain ranges of the external bias potential thanks to their intrinsic broken inversion symmetry configuration with spontaneous charge transfer. In Fig. 5 we present the total energies of the different types of solutions in the low bias regime, obtained by starting the self-consistent calculations from different seeds. For low potential bias the charge balanced AF structure remains lowest in energy. Eventually the external field becomes large enough to flip the layer polarization of one valley-spin component towards the layer favored by the electric field, giving rise to the Fi type solutions. The electrostatic charge imbalance of the Fi states is approximately half of that associated with the F state in which all four components are polarized towards the same layer, a fact that can be inferred from the slopes of the total energy evolution as a function of external electric field. In Fig. 6 we present the charge densities associated with one valley-spin component with different layer polarizations. For the AF and Fi solutions we have components that are polarized toward both layers that we represent as $\Delta n_l = (n_l - n_0)$, the density difference with respect to the uniform background density n_0 . In the Fi configuration the three charge density components polarized towards the same layer do not have exactly the same value when the electron spins are different, but they are similar in magnitude. In the F configuration all four density components are polarized towards the same layer and have the same magnitude.

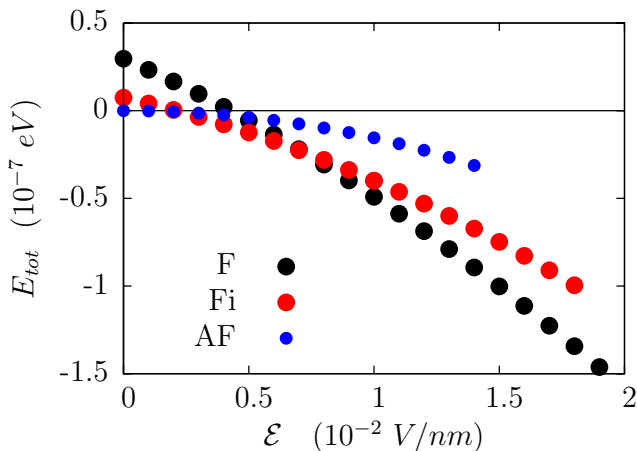


FIG. 5: Bias dependence of the total energies of the system for different valley-spin polarization configurations for a system with $\epsilon_r = 4$. The system undergoes transitions from the AF to Fi and then to F states as a function of external field, each one displaying clearly different quantum Hall conductivity properties. The origin of energy has been arbitrarily shifted for presentation convenience.

The behavior of the band gaps in the low bias regime illustrates the character of each solution. The AF band gap continually decreases when the electric field is increased. In this case the electric field always works against the charge density distribution of two components directly contributing in the reduction of the band gap. For the F configuration we have a completely opposite trend; the gap always increases since the electric field favors charge accumulation in the layer in which the density is already higher. In the Fi configuration we find an intermediate situation. We find an initial increase of the gap in presence of an electric field thanks to the reduction of the Hartree energy penalty associated to the spontaneous charge imbalance. Beyond a certain point the band gap starts to decrease, reflecting the fact that the electric field is working against the layer polarization of one component. Eventually when the effect of the external field becomes dominant the system undergoes a phase transition to the F configuration. Every time there is a crossover of the minimum energy levels we will see an abrupt change in the band gap and charge density. The Hall conductivity of the system will also see discontinuous changes following the classification of table I. The observations above suggest that the band gap will show a non-monotonic dependence on potential bias with an initial reduction at low fields for AF states and an increase for large enough bias for F states. Between those two limits the system can form a Fi state that also has a band gap that decreases with increasing electric field, before finally making a transition to the F state.

D. Exchange screening effects in presence of a strong bias

In the presence of an external bias the inversion symmetry of graphene bilayer is explicitly broken, favoring the charge

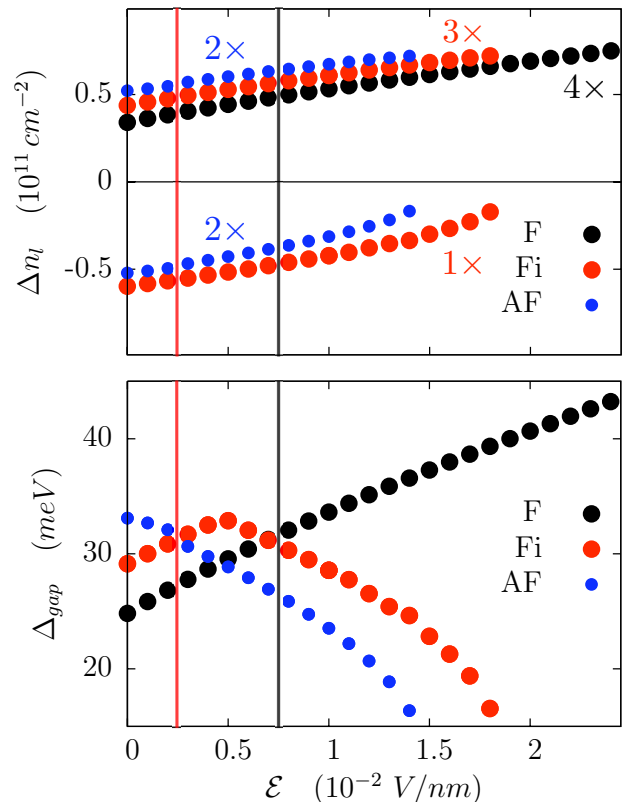


FIG. 6: *Upper panel:* Each branch represents the bias dependence of the valley resolved layer polarization density associated with one valley-spin component. These results were obtained for a system with $\epsilon_r = 4$. The multiplication factors represent the number of times each branch needs to be repeated to give the total charge density to complete the contributions from the four components. *Lower panel:* Band gap as a function of bias for F, Fi and AF states for a system with $\epsilon_r = 4$. We observe a competition in the band-gap opening between exchange and Hartree contributions which can lead to a reduction of the band gap as the bias is increased.

accumulation in one of the layers and opening a band gap, a fact that has been verified in several experiments^{35–37} and also predicted theoretically within tight-binding³⁸, tight-binding plus Hartree screening^{39,40} or ab-initio calculations¹⁵. Here we explore the role that electron exchange can play when the system is subject to a strong external bias. In Fig. 7 we present the charge accumulation in one of the layers as a function of bias. In the strong bias limit we are in the F configuration in which all four components are polarized towards the same layer. Results obtained in the Hartree approximation follows a similar trend in the strong bias limit resulting in comparable amounts of total transferred charge in the range of bias we considered, with the Hartree only screening allowing more sloshed charge. A larger value of dielectric screening ϵ_r that weakens the interaction strength also weakens the electrostatic screening and therefore more charge imbalance per layer is expected.

As we show in Fig. 7 the presence of the exchange term in

the Hamiltonian introduces a clear enhancement of the band gap that persists up to high bias potentials. This gap enhance-

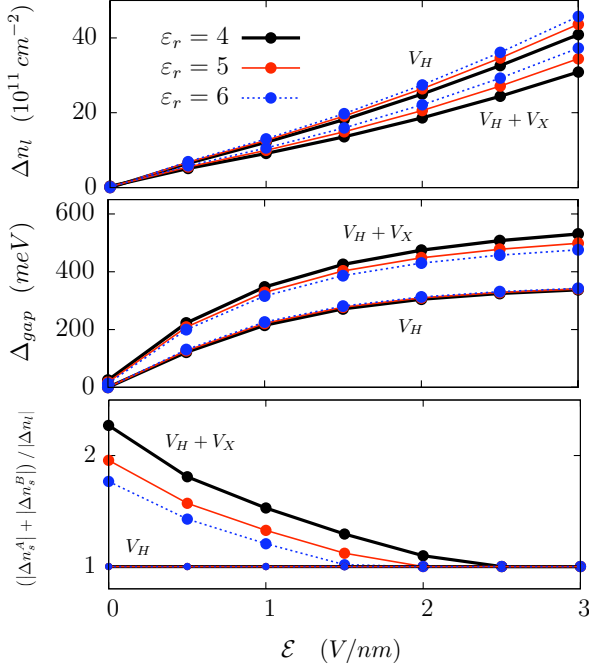


FIG. 7: External bias dependence of layer resolved charge density, band gaps and sublattice charge asymmetry. We have considered the F configuration where all four valley-spin components are polarized towards the same layer. *Upper panel*: Charge accumulation dependence as a function of bias in presence of Hartree and Fock terms and charge accumulation dependence as a function of bias in presence of Hartree screening only. The evolution of Δn_l as a function of bias has a slightly larger slope in the Hartree only approximation than the Hartree-Fock case. *Middle panel*: Band gaps obtained for Hartree-Fock and Hartree approximations using different values of ϵ_r as a function of external electric field \mathcal{E} . We notice a substantial enhancement of the band gap when the exchange term is included. *Lower panel*: Measure of deviation from neutrality in the charge differences for each one of the sublattices in a given layer normalized by the total sloshed charge. The asymmetric distribution of the charge between low energy sublattice A and high energy sublattice B of a given graphene layer is enhanced in presence of electron exchange. This asymmetry becomes smaller as the external bias becomes stronger.

ment can be related to the exchange contribution that tends to introduce a strong asymmetry in charge distribution between A and B sublattices of a given layer that persists up to rather high values of external electric field as shown in Fig. 7. We may define this intralayer charge imbalance ratio as $(|\Delta n_s^A| + |\Delta n_s^B|) / |\Delta n_l|$. The enhancement of charge imbalance between the sublattices is one of the effects of intralayer exchange that contributes to changing the magnitude of the band gap. This quantity is more sensitive to the strength of the Coulomb interaction than to changes in the temperature.

V. SUMMARY AND CONCLUSIONS

We have presented a numerical description of the broken charge symmetry Hartree-Fock ground state in a graphene bilayer system for different dielectric screening of the media and temperature. The predicted gap sizes and temperature ranges in which this effect is expected to survive should be experimentally accessible. The size of the interlayer charge transfers suggests that the broken symmetry states will be suppressed by smooth disorder strong enough to produce charge puddles with density variations larger than around 10^{-5} per carbon atom. The total amount of spontaneous charge transfer from one layer to another in the broken ground state is $\sim 10^{11} \text{cm}^{-2}$, smaller but comparable in magnitude to the densities that can be induced by gating the device or depositing impurities¹ and can therefore be relevant for interpreting gating experiments in bilayer graphene. The mechanism for broken symmetry described here is most effective for a neutral bilayer because the energy gain due to charge transfer is greatest for electrons nearest to the Dirac point. The broken symmetries are expected to be present only when the carrier density is smaller than about 10^{11}cm^{-2} , hence a reduction of this effect is expected as the Fermi surface moves away from the charge neutrality point when the system is doped.

The Coulomb correlation neglected in the Hartree-Fock formalism usually plays a more important in extended systems⁴¹ than in localized atomic systems where they are typically one order of magnitude smaller than exchange effects. Treatments of Coulomb correlation based on a renormalization group framework⁸ or RPA²³ suggest that the broken symmetry addressed in this paper will survive when Coulomb correlation is considered. In our case we have used larger values of ϵ_r than those based on estimates from dielectric functions alone in order to effectively reduce the strength of exchange to approximately account for screening effects. Application of a self-consistent dynamic screening approximation to this problem would be interesting but would require the high density of sampling k -points near the Dirac point to be implemented in a computationally efficient way.

An interesting feature of these broken symmetry states is the spontaneous quantum Hall effects which appear when opposite valleys have opposite layer polarizations.¹⁰ When opposite valleys have the same layer polarization, the system has only a valley Hall effect, which is not manifested in standard electrical measurements. There is no energy difference between these states in a continuum model which does not account for lattice-scale physics. We find that the energy difference between these states decreases rapidly depending on the strength of the on-site effective interaction in our π -band only model, with valley Hall states being favored over anomalous Hall states. For a very weak on site interaction, anomalous Hall states could be favored over valley Hall states. States in which electrons with one spin orientation form one Hall state, while electrons with the other spin form the other Hall state also occur. Despite the uncertainties of the calculation due to this high sensitivity to lattice details they do give us an estimate for the magnitude of the energy differences between different configurations. Unlike Nandkishore and Levitov,⁹

we find that valley Hall states have lower energy than anomalous Hall states, but that the energy competition can be altered by even quite weak external magnetic fields. This scenario appears to be consistent with experiments from the Yacoby group in which a $\nu = 4$ quantized Hall effect persists down to very weak magnetic fields. The small energy differences between competing states could mean that domains with all characters are present, separated by domain walls, because of entropic and disorder considerations. In the presence of a magnetic field, coupling of spontaneous orbital magnetism to the external field favors anomalous Hall states and should coarsen any domain structure. Similarly an externally applied potential bias favors valley Hall states and should also coarsen domain structures. In the absence of disorder we do find that the charge gap is first decreased by potential bias, and finally increased once both spins have valley Hall effects with the same layer polarization. This finding is qualitatively consistent with experiment.¹³

We have also presented mean field theory estimates of the

critical temperatures associated with spontaneous layer polarization states in graphene bilayers. According to these estimates, order will not survive to room temperatures and therefore is unlikely to be useful for applications. On the other hand, the exchange interactions which produce broken symmetry states at low temperatures, will still play a role in enhancing gaps produced by external potential biases at room temperature.

Acknowledgments

We gratefully acknowledge discussions with Hongki Min, Marco Polini, Byounghak Lee, Wang Yao, Rahul Nandkishore, Dagim Tilahun and Andrea Young. Financial support was received from Welch Foundation grant TBF1473, NRI-SWAN, DOE grant Division of Materials Sciences and Engineering DE-FG03-02ER45958.

-
- * Electronic address: jeil@physics.utexas.edu
- ¹ K. S. Novoselov, A. K. Geim, S. V. Morozov, D. Jiang, M. I. Katsnelson, I. V. Grigorieva, S. V. Dubonos, and A. A. Firsov, *Nature (London)* **438**, 197 (2005).
 - ² Y. Zhang, Y.-W. Tan, H.L. Stormer, and P. Kim, *Nature* **438**, 201 (2005).
 - ³ A. K. Geim and K. S. Novoselov, *Nature Mat.* **6**, 183 (2007); A. K. Geim and A. H. MacDonald, *Phys. Today* **60**, 35 (2007).
 - ⁴ Y. Barlas *et al.*, *Phys. Rev. Lett.* **98**, 236601 (2007).
 - ⁵ S. Das Sarma, E. H. Hwang, and W.-K. Tse, *Phys. Rev. B* **75**, 121406(R) (2007); E. H. Hwang, Ben Yu-Kuang Hu, and S. Das Sarma, *Phys. Rev. B* **76**, 115434 (2007); F. Guinea, A. H. Castro Neto, and N. M. R. Peres, *Eur. Phys. J. Special Topics* **148**, 117-125 (2007); J. Nilsson, A. H. Castro Neto, N. M. R. Peres, and F. Guinea, *Phys. Rev. B* **73**, 214418 (2006).
 - ⁶ Edward Mc Cann and Vladimir I. Fal'ko *Phys. Rev. Lett.* **96**, 086805 (2006).
 - ⁷ H. Min, G. Borghi, M. Polini and A. H. MacDonald, *Phys. Rev. B* **77**, 041407(R) (2008).
 - ⁸ F. Zhang, H. Min, M. Polini, and A. H. MacDonald, *Phys. Rev. B* **81**, 041402(R) (2010).
 - ⁹ R. Nandkishore and L. Levitov, *Phys. Rev. B* **82**, 115124 (2010); arXiv:1002.1966 (2010).
 - ¹⁰ F. Zhang *et al.*, to be published (2010).
 - ¹¹ D. Xiao, M.-C. Chang and Q. Niu, *Rev. Mod. Phys.* **82**, 1959 (2010).
 - ¹² N. Nagaosa, J. Sinova, S. Onoda, A. H. MacDonald, and N. P. Ong, *Rev. Mod. Phys.* **82**, 15391592 (2010).
 - ¹³ R. T. Weitz, M. T. Allen, B. E. Feldman, J. Martin and A. Yacoby, *Science* Vol. 330 no. 6005 pp. 812-816; J. Martin, B. E. Feldman, R. T. Weitz, M. T. Allen and A. Yacoby, arXiv:1009.2069 (2010); R. T. Weitz, M. T. Allen, B. E. Feldman, J. Martin and A. Yacoby, arXiv:1010.0989 (2010).
 - ¹⁴ S.H. Abedinpour, M. Polini, A.H. MacDonald, B. Tanatar, M.P. Tosi, and G. Vignale, M.P. Tosi, and G. Vignale, *Phys. Rev. Lett.* **99**, 206802 (2007); **99**, 206802 (2007). J.B. Oostinga *et al.*, *Nature Mat.* **7**, 151 (2008); J. Martin, *Bull. Am. Phys. Soc.* **54**, 191 (2009); Pablo San-Jose, Elsa Prada, Edward McCann, and Henning Schomerus, *Phys. Rev. Lett.* **102**, 247204 (2009).
 - ¹⁵ H. Min, B. Sahu, S. K. Banerjee, and A. H. MacDonald, *Phys. Rev. B* **75**, 155155 (2007).
 - ¹⁶ J. W. McClure, *Phys. Rev.* **108**, 612 (1957).
 - ¹⁷ B. Partoens and F. M. Peeters, *Phys. Rev. B* **74**, 075404 (2006).
 - ¹⁸ Attila Szabo and Neil Ostlund, 'Modern Quantum Chemistry: Introduction to Advanced Electronic Structure Theory' Dover (1996).
 - ¹⁹ G. Dresselhaus, *Phys. Rev. B* **10**, 3602 (1974).
 - ²⁰ E. McCann and V. I. Falko, *Phys. Rev. Lett.* **96**, 086805 (2006).
 - ²¹ O. Vafek and K. Yang, *Phys. Rev. B* **81**, 041401(R) (2010).
 - ²² K. Sun, H. Yao, E. Fradkin, and S. A. Kivelson, *Phys. Rev. Lett.* **103**, 046811 (2009).
 - ²³ R. Nandkishore and L. Levitov, *Phys. Rev. Lett.* **104**, 156803 (2010).
 - ²⁴ G. Borghi, M. Polini, R. Asgari, A.H. MacDonald, *Phys. Rev. B* **82**, 155403 (2010).
 - ²⁵ G. Borghi, M. Polini, R. Asgari, and A.H. MacDonald, *Solid State Commun.* **149**, 1117 (2009).
 - ²⁶ For unbiased bilayers, states in which layer polarization occurs in combination with coherence between different valleys are degenerate with states in which various layer polarizations occur within a valley. In a lattice model, coherence between valleys implies a charge-density-wave structure in the broken symmetry state which is not permitted in the class of states we examine. Although we believe that these states will have higher energies because of associated electrostatic energy increases, particularly so when an interlayer bias is present, they should be examined more closely in future work.
 - ²⁷ D. Xiao, W. Yao and Q. Niu, *Phys. Rev. Lett.* **99** 236809 (2007).
 - ²⁸ D. J. Thouless, M. Kohmoto, M. P. Nightingale, and M. den Nijs, *Phys. Rev. Lett.* **49**, 405 (1982).
 - ²⁹ M.-C. Chang and Q. Niu, *Phys. Rev. B* **53**, 7010 (1996).
 - ³⁰ W. Yao, D. Xiao and Q. Niu, *Phys. Rev. B* **77**, 235406 (2008).
 - ³¹ E. Prada, P. San-Jose and L. Brey, arXiv:1007.4910v1 (2010).
 - ³² J. Li, I. Martin, M. Buttiker, A. F. Morpurgo, arXiv:1009.4851 (2010); I. Martin, Y. M. Blanter, A. F. Morpurgo, *Phys. Rev. Lett.* **100**, 036804 (2008).
 - ³³ J. Jung and A. H. MacDonald, *Phys. Rev. B* **80**, 235417 (2009).
 - ³⁴ J. Jung, to be published.

- ³⁵ T. Ohta, A. Bostwick, T. Seyller, K. Horn, and E. Rotenberg, *Science* **313**, 951 (2006).
- ³⁶ J. B. Oostinga, et al. *Nature Materials* **7**, 151 (2007).
- ³⁷ Y. Zhang, T.-T. Tang, C. Girit, Z. Hao, M. C. Martin, A. Zettl, M. F. Crommie, Y. R. Shen and F. Wang, *Nature* Vol. **459**, 820 (2009)
- ³⁸ E. V. Castro, K. S. Novoselov, S. V. Morozov, N. M. R. Peres, J. M. B. Lopes dos Santos, J. Nilsson, F. Guinea, A. K. Geim, and A. H. Castro Neto, *Phys. Rev. Lett.* **99**, 216802 (2007).
- ³⁹ E. McCann, *Phys. Rev. B* **74**, 161403(R) (2006).
- ⁴⁰ L. M. Zhang, Z. Q. Li, D. N. Basov, M. M. Fogler, Z. Hao and M. C. Martin, *Phys. Rev. B* **78**, 235408 (2008); L. A. Falkovsky, *Phys. Rev. B* **80**, 113413 (2009).
- ⁴¹ C. Attaccalite et al. *Phys. Rev. Lett.* **88**, 256601 (2002); *Phys. Rev. Lett.* **91**, 109902(E) (2003).
- ⁴² E. Rossi, S. Das Sarma, *Phys. Rev. Lett.* **101**, 166803 (2008).
- ⁴³ J. C. Slater, *Phys. Rev.* **81**, 385390 (1951); A. Seidl, A. Görling, P. Vogl, J. A. Majewski, and M. Levy, *Phys. Rev. B*, **53** 3764 (1996).
- ⁴⁴ W.-K. Tse and A. H. MacDonald, *Phys. Rev. Lett.* **105**, 057401 (2010).